RSC Advances

PAPER

View Article Online
View Journal | View Issue

Cite this: *RSC Adv.*, 2021, **11**, 30383

Stable cycling of Prussian blue/Zn battery in a nonflammable aqueous/organic hybrid electrolyte†

Zheng Xu,‡[a] Bo Xiang,[b] Chunli Liu,‡[a] Yunpo Sun,[a] Jian Xie,*[a] Jian Tu,[c] Xiongwen Xu[c] and Xinbing Zhao[a]

Received 13th July 2021
Accepted 7th September 2021

DOI: 10.1039/d1ra05369h

rsc.li/rsc-advances

Although rechargeable aqueous batteries are attracting increasing attention in recent years due to high safety, low cost, high power density and environmental friendliness, the aqueous batteries suffer from limited cycle life due to a narrow electrochemical window of the aqueous electrolytes, severe side reaction and instability of electrode materials in aqueous electrolytes. In this work, we propose a hybrid aqueous electrolyte with a mixed solvent of water and acetonitrile (ACN), which exhibits a wide electrochemical window, high ionic conductivity, and nonflammability. An aqueous battery with an iron hexacyanoferrate (FeHCF) cathode, Zn anode and H_2O/ACN hybrid electrolyte shows a high capacity of 69.1 mA h g^{-1} at 10C (89.5% relative to that at 1C) and an extremely long cycle life with 51.4% capacity retention after 19 000 cycles at 10C. The excellent cycling performance of the aqueous FeHCF/Zn batteries can be attributed to the reduced water activity and extended electrochemical window because of the strong hydrogen-bonding interaction between ACN and H_2O. Besides, the large particle size and good crystallization of FeHCF can inhibit its dissolution in the aqueous electrolyte which further improves cycling performance. This work will shed light on the design of safe aqueous batteries for applications in large-scale energy storage.

1. Introduction

With the increasing demands of energy and the dwindling supplies of traditional fossil fuels such as coal, petroleum and natural gas, the storage and use of renewable energy is becoming increasingly important nowadays. However, the variability of the renewable energy prevents it from integrating into the electric grid directly, which limits its efficient use. Therefore, developing large-scale energy storage systems (EESs) is essential for utilization of the renewable energy in a stable and effective manner.[1–3] Sodium-ion batteries (SIBs) are considered to be a suitable choice for stationary energy storage system due to the resource abundance of Na.[4,5] However, the volatile, flammable, and toxic features of the organic electrolytes will bring potential safety and environment concerns for organic SIBs.[6] In this regard, it is necessary to develop safe and environmentally friendly SIBs suitable for grid-scale applications.

The aqueous Daniell-type sodium-based hybrid ion battery is an ideal choice with merits of non-flammability, low cost, high power density, environmental benignity and easy assembly by using a metal anode directly.[7] Different from the rocking-type SIBs, the Daniell-type sodium-based hybrid ion batteries work with Na^+ insertion into/extraction from the cathode and Zn^{2+}, Mg^{2+} or Al^{3+} deposition on/stripping from the anode.[8–10] However, owing to the high activity of free H_2O in aqueous electrolyte, Daniell-type batteries like $Na_2MnHCF\|Zn$,[11] $Na_{0.44}MnO_2\|Zn$[12] and $NiHCF\|Zn$[13] usually exhibit an unsatisfied cycle life because of dissolution/decomposition of the cathode and corrosion of metal anode. Besides, aqueous electrolyte with free H_2O of high activity can lead to a narrow electrochemical stability window of ~1.23 V, which limits both battery energy density and selection of electrode materials, and water decomposition outside the electrochemical window will result in a low coulombic efficiency, battery swelling, and electrolyte deterioration.[14–16] In order to address the high activity of free H_2O in the aqueous electrolytes, super-concentrated aqueous electrolytes have been proposed, so as to suppress water activity by forming "water-in-salt" or "hydrate-salt" structure to eliminate the free H_2O.[17–19] For example, Wang *et al.* reported a super-concentrated aqueous electrolyte of 21 M

[a]*State Key Laboratory of Silicon Materials, School of Materials Science and Engineering, Zhejiang University, Hangzhou 310027, P. R. China. E-mail: xiejian1977@zju.edu.cn; Fax: +86-571-87951451; Tel: +86-571-87952181*

[b]*Huayou New Energy Technology (Quzhou) Co., Ltd., Quzhou 324000, P. R. China*

[c]*LI-FUN Technology Corporation Limited, Zhuzhou 412000, P. R. China*

† Electronic supplementary information (ESI) available: Comparison of cycling performance and rate capability of various battery systems and the related references, and gas evolution experiment of the aqueous battery in the idle mode. See DOI: 10.1039/d1ra05369h

‡ Zheng Xu and Chunli Liu contributed equally to this work.

lithium bis(trifluoromethane sulfonyl)imide (LiTFSI), which showed a wide electrochemical window of ~3 V.[20] Lee *et al.* proposed a super-concentrated aqueous electrolyte of 17 M $NaClO_4$ with an electrochemical window of ~2.7 V.[21] However, super-concentrated electrolytes generally suffer from low ionic conductivity and high viscosity due to the strong interactions between anions and cations. Besides, the use of large amounts of expensive salts also impedes the practical applications of super-concentrated electrolyte. Another useful method is to use "localized high concentration" electrolytes, where a cosolvent that cannot dissolve the salt is added to dilute the electrolyte. In this way, the overall salt concentration is controlled at a reasonable value while the property of super-concentrated electrolyte is maintained in local environment. Besides, the viscosity and cost can be effectively reduced because of lower salt content, which provides a practical way for design of advanced aqueous energy storage system.[22–24] In addition to the use of high (or localized high) concentration electrolytes, some organic additives, such as ethylene glycol (EG),[25] poly(ethylene glycol) (PEG),[26] dimethyl sulfoxide (DMSO),[27] were used to extend the electrochemical window of the aqueous electrolytes. The strong hydrogen-bonding interactions between water and organic solvent occur to change the solvation structure of cations with water and break the original hydrogen-bond network of water with reduced activity of water. As a result, batteries with the water–organic additive-salt hybrid system exhibit an obviously extended electrochemical window and thereby a long cycle life.

Previous reports showed that the addition of acetonitrile (ACN) can reduce the activity of free water and build a protective interface on Zn anode, thus enhancing the cycling performance of the aqueous batteries.[28] Yan *et al.* found that ACN is suitable organic cosolvent for hybrid electrolyte that possesses superior wettability, enables fast ion diffusion and has a wide electrochemical window.[29] In addition, H_2O and ACN are intersoluble with easy adjusting of ACN ratio. Inspired by those facts, in this work, we report an aqueous Daniell-type battery with iron hexacyanoferrate (FeHCF) cathode, metallic Zn anode, and a hybrid aqueous electrolyte. The hybrid aqueous electrolyte is composed of a mixed ACN/H_2O solvent, 1 M $NaCF_3SO_3$ (NaTfO) and 0.1 M $Zn(CF_3SO_3)_2$ ($Zn(TfO)_2$), where the ratio of ACN and water is optimized to achieve a comprehensive performance of nonflammability, wide voltage window, low viscosity and acceptable ionic conductivity. The results show that the ACN can form strong hydrogen-bonding interaction with water to extend electrochemical windows and restrain the side reaction of the aqueous electrolyte. In addition, the hybrid electrolyte with 50 wt% ACN addition exhibits the best comprehensive performance (low viscosity, wide electrochemical window, high conductivity and nonflammability) and the structure of FeHCF cathode can be well preserved after long-term cycling in this hybrid aqueous electrolyte. Electrochemical tests show that the aqueous FeHCF||Zn battery with such a hybrid electrolyte exhibits an ultralong cycle life at a high current density.

2. Experimental section

2.1 Material preparation

The FeHCF material was synthesized by a facile coprecipitation method as previously reported.[30] Briefly, 50 mL of 0.06 M $Na_4Fe(CN)_6$ solution and 50 mL of 0.09 M $FeSO_4$ solution with 1.4 g ascorbic acid and 20 g sodium citrate were added dropwise into 100 mL of deionized (DI) water simultaneously at a feeding speed of 1 mL min^{-1} with bubbled N_2 at 25 °C. The suspension was then aged for 4 h to complete the reaction. Finally, the FeHCF was obtained by centrifugal separation and drying at 100 °C for 24 h in vacuum.

2.2 Electrode and electrolyte preparation

The Na_xFeHCF cathodes were prepared by pasting the slurry composed of 70 wt% active material (FeHCF), 20 wt% Ketjen black (KB) conductive agent and 10 wt% polyvinylidene fluoride (PVDF) binder onto titanium foil followed by drying under vacuum at 80 °C for 12 h. The zinc anode was prepared by covering a polyamide layer on the surface of zinc foil according to the reported method.[31] The polyamide film was used to protect Zn from corrosion. A series of hybrid electrolytes were prepared by dissolving 1 mol NaTfO and 0.1 mol $Zn(TfO)_2$ in 1 kg hybrid ACN/DI water solvent with an ACN weight ratio of 0%, 25%, 50%, 75% and 90%, respectively.

2.3 Materials characterization

X-ray diffraction (XRD) patterns were acquired on a Rigaku D/Max-2550pc powder diffractometer with Cu Kα radiation (λ = 1.541 Å). The morphologies of the powder samples and electrodes were observed by field-emission scanning electron microscopy (SEM) on a Hitachi (Japan) S-4800 microscope. The viscosity of the hybrid electrolytes was measured by rotational rheometer (HAAKE-RS6000) at 25 °C with a shear rate of 1–1000 s^{-1}. Nuclear Magnetic Resonance (NMR) spectroscopy was measured on an Agilent DD2 600 device at 25 °C, where deuterated H_2O (D_2O) was used as the field frequency lock and the mass fraction of D_2O is fixed at 20 wt%.

2.4 Electrochemical measurements

Linear Sweep Voltammetry (LSV) was conducted on a VersaSTAT3 electrochemical workstation (Princeton Applied Research) in a three-electrode system with Ti foil as the working electrode, platinum electrode as the counter electrode, and Ag/AgCl electrode as the reference electrode. The hybrid electrolytes were purged with nitrogen to remove the dissolved oxygen. The ionic conductivity of the hybrid electrolytes was measured by AC impedance method and calculated by the equation:

$$\sigma = \frac{L}{R_s A}$$

where σ is ionic conductivity, R_s is electrolyte impedance, A is the area of Pt sheet and L is distance between two parallel-placed Pt sheets (1 cm × 1 cm) immersed in the electrolytes.

The coin-type FeHCF/Zn full cells were assembled using the hybrid electrolyte, FeHCF cathode, Zn anode (30 μm thickness) and glass fiber membrane separator. Galvanostatic cycling of the FeHCF/Zn cells was conducted on a cell cycler (Neware Technology Ltd, China) with a cut-off voltage of 0.6 and 1.5 V (*vs.* Zn/Zn^{2+}), where the specific capacity and current density were normalized according to the weight of FeHCF. Electrochemical Impedance Spectroscopy (EIS) was measured on the VersaSTAT3 workstation with an AC voltage of 10 mV amplitude at frequency of 10^{-2} to 10^{5} Hz. All the electrochemical measurements were conducted at room temperature.

3. Results and discussion

The FeHCF was synthesized by a facile coprecipitation method as shown in Fig. 1a. The sodium citrate acts as chelating agent to control coprecipitation rate and the ascorbic acid acts as reducing agent to prevent Fe^{2+} oxidation.[32] With this method, well crystallized, micro-sized FeHCF can be obtained. XRD patterns of the FeHCF was shown in Fig. 1b. The remarkably split peaks at around 25° (2θ) indicate that the FeHCF has a monoclinic structure. SEM images in Fig. 1c exhibit that the sample exhibits a cubic-shaped, border-rich morphology with a particle size of 2–3 μm. Fig. 1d shows the appearance of the

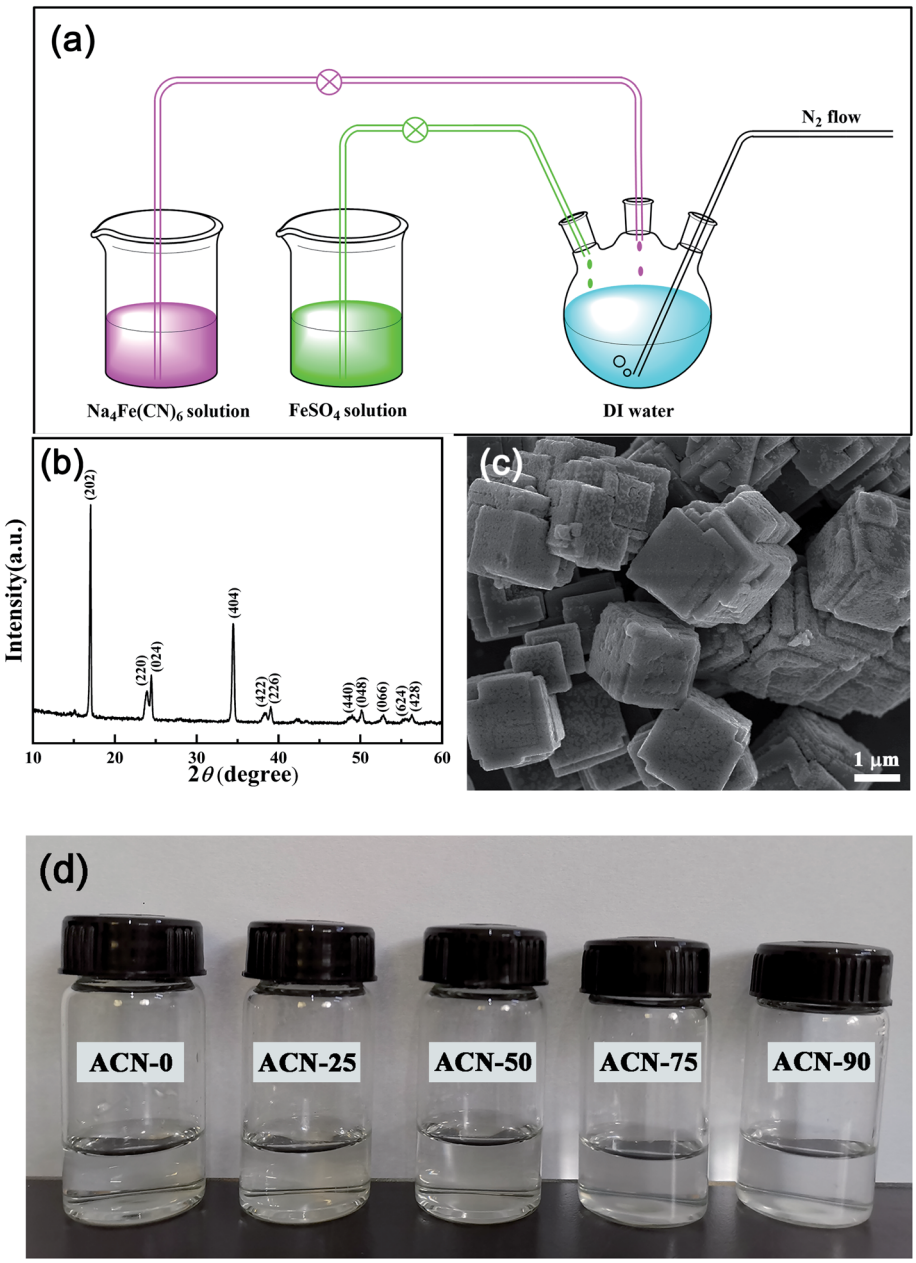

Fig. 1 (a) Schematic illustrate of preparation process of FeHCF, (b) XRD patterns and (c) SEM images of FeHCF, and (d) appearance of the hybrid electrolytes with various ACN/H_2O ratios.

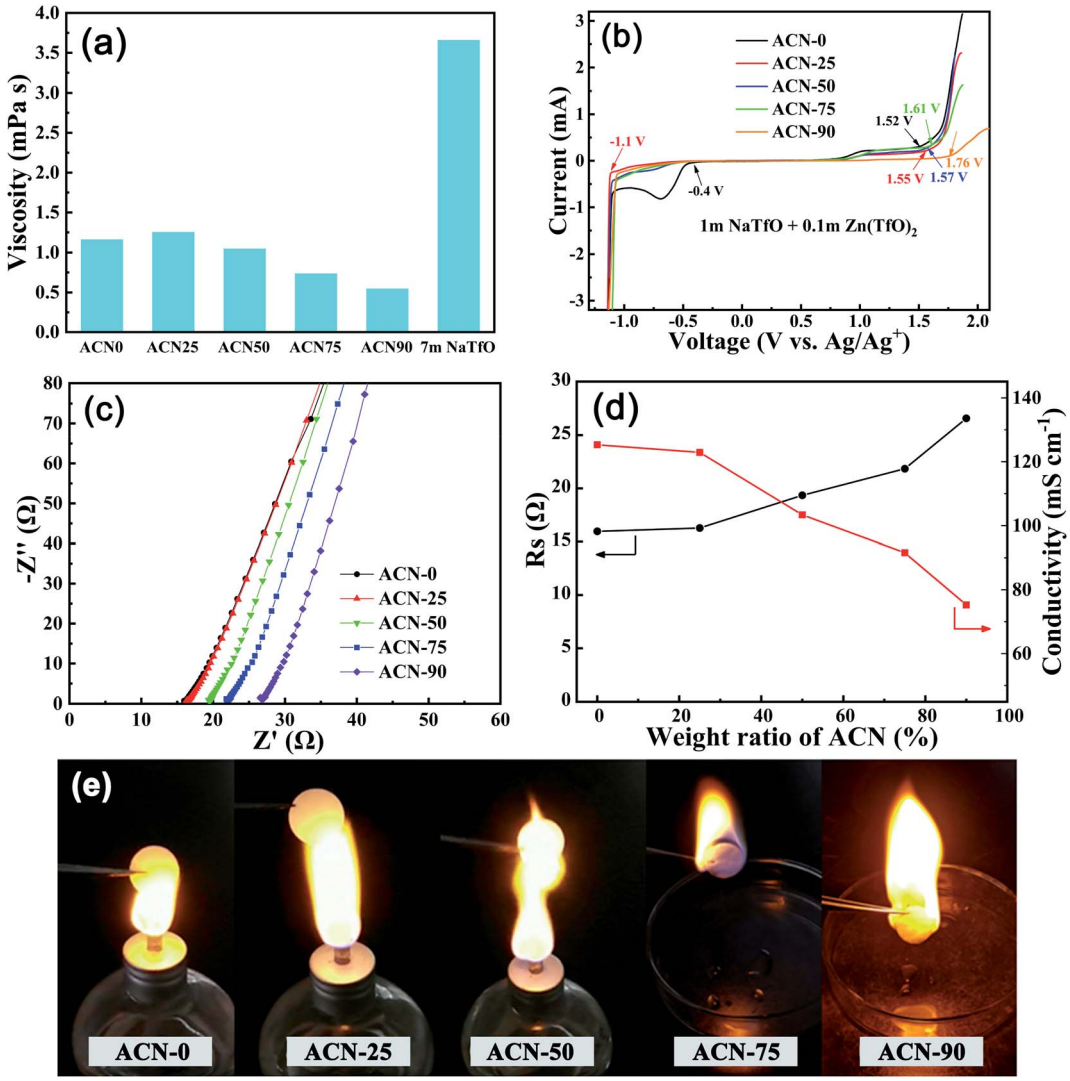

Fig. 2 Physicochemical performance tests of the hybrid electrolytes with different ACN ratios: (a) viscosity, (b) LSV scanning, (c) EIS, (d) ionic conductivity, and (e) flammability.

hybrid electrolytes of 1 M NaTfO and 0.1 M $Zn(TfO)_2$ in a mixture of H_2O and ACN, where the mass ratios of ACN are 0% to 25%, 50%, 75%, and 90 wt%, and the samples are labeled as ACN-0, ACN-25, ACN-50, ACN-75 and ACN-90, respectively. Note that H_2O and ACN are intersoluble forming transparent solutions.

Fig. 2 compares the physicochemical properties of the hybrid electrolytes with different ACN ratios. As shown in Fig. 2a, the hybrid electrolytes with a normal salt concentration exhibit a significantly lower viscosity than the 7 M NaTfO electrolyte. The viscosity of the electrolyte increases first and then decreases with the increasing proportion of ACN. At a low ACN content (<25 wt%), the viscosity increase is attributed to the molecular interactions between ACN and H_2O, where the cations are surrounded mainly by the water molecules. With an increase in ACN proportion, some water molecules around the cations are replaced by the ACN molecules and distance between anions and cations are enlarged because of the larger molecule size of ACN, with weakened ionic interactions overwhelming the strengthened molecular interaction and thereby reduced viscosity.[25] Fig. 2b shows the electrochemical windows of the hybrid electrolytes measured by LSV, where the oxygen evolution potential gradually increases from 1.52 to 1.76 V (*vs.* Ag/AgCl) as the ACN ratio increases from 0 to 90 wt%. Similarly, the hydrogen evolution is also suppressed by adding ACN with hydrogen evolution potential shifted from −0.4 V to −1.1 V (*vs.* Ag/AgCl). Note that the bump near −0.7 V *vs.* Ag/Ag^+ is attributed to bubble formation on the Ag/AgCl electrode.[21] The results suggest that ACN addition can inhibit the water decomposition by decreasing the free water amount. The difference in the peak at 1.0 V between ACN-90 and other electrolytes is ascribed to the significantly different solvation structure of ACN–H_2O system, where the hydrogen-bonding interaction among H_2O are almost destroyed for ACN-90, thus resulting in obviously extended electrochemical stability windows of ACN-90.[33] Fig. 2c shows the EIS of the hybrid electrolytes, where the intercept on the real

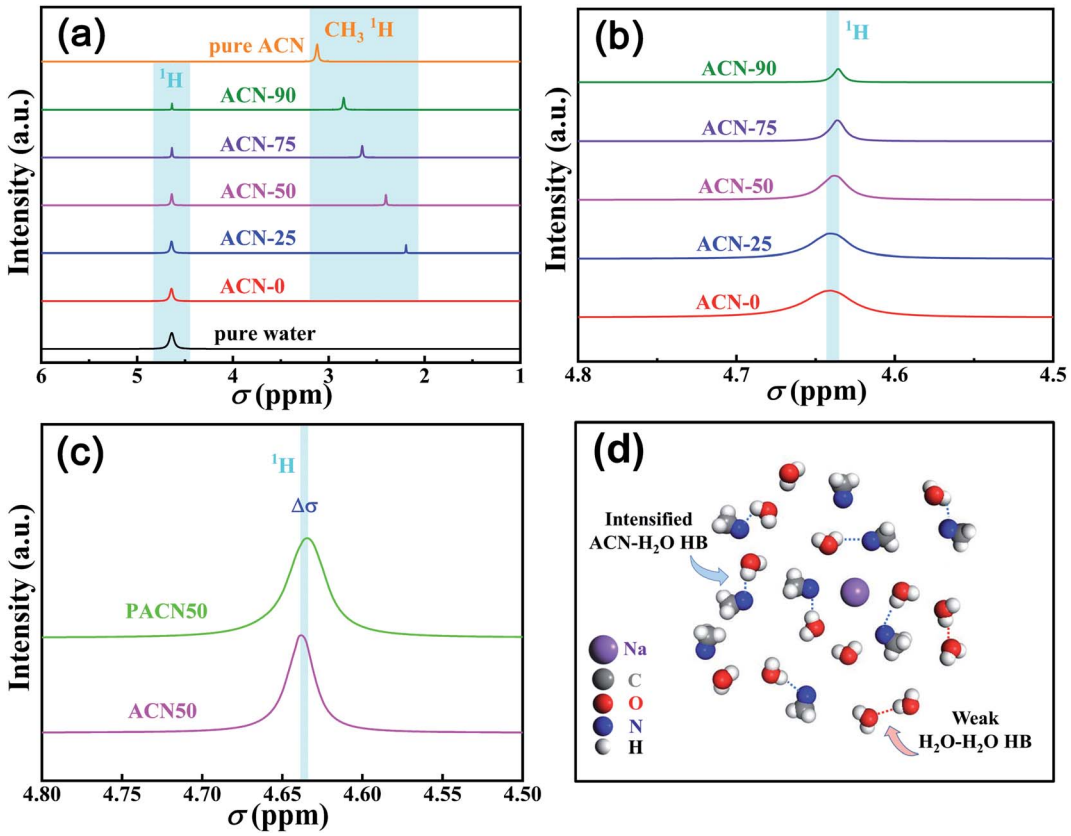

Fig. 3 (a) ^{1}H NMR spectra of a series of the ACN/H_2O hybrid electrolytes at 25 °C, (b) ^{1}H NMR spectra from H_2O of the hybrid electrolytes, (c) comparison of ^{1}H NMR spectra from H_2O of the salt-added ACN-50 and salt-free PACN, and (d) schematic illustration of proposed structure of the hybrid electrolytes.

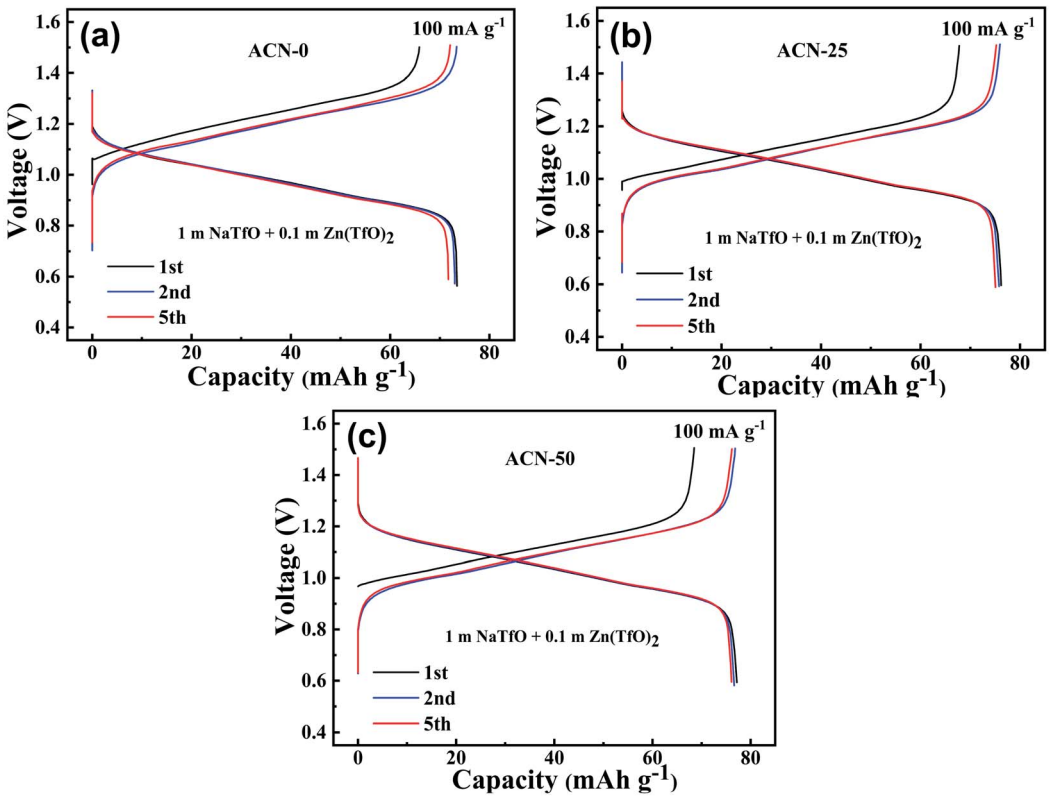

Fig. 4 Charge/discharge curves of aqueous batteries with various the electrolytes: (a) ACN-0, (b) ACN-25, and (c) ACN-50.

axis (R_s) is used to calculated the ionic conductivity of the hybrid electrolytes (Fig. 2d). The ionic conductivity exhibits a downward trend due to the increased solvated ion size as the ACN content increases. Fig. 2e demonstrates flammability tests of the hybrid electrolytes. Note that the hybrid electrolytes are nonflammable when the proportion of ACN is below 50%. This indicates that nonflammability can be achieved even at a relatively high organic solvent ratio.

In order to understand the effect of the ACN addition on extending the voltage window of the hybrid electrolytes, NMR tests were conducted as shown in Fig. 3. The ^{1}H resonance from OH of pure water (H_2O) is at 4.641 ppm which is almost the same as that of ACN-0 electrolyte, indicating that the hydrogen-bonding (HB) network of the aqueous electrolyte without ACN is almost the same as that of pure water (without salts). After adding 25 wt% ACN, the ^{1}H peak of H_2O moves to higher field with a smaller σ value and it continually moves to higher field with increasing ACN content and finally reaches 4.636 ppm in ACN-90 sample (Fig. 3a and b). These results indicate that the electron density of ^{1}H from H_2O increases as the ACN content increases which is due to the hydrogen-bonding interaction between ACN and water, namely, the relatively weak hydrogen bonds among water molecules are broken and stronger hydrogen bonds between ACN and water molecules form. The enhanced hydrogen-bonding interaction of ACN–H_2O reduces the activity of H_2O and results in an extended electrochemical stability window, which can also be verified by the opposite shift of ^{1}H from CH_3 with increasing ACN ratio.[34] In order to clarify the effect of salt addition on hydrogen-bonding interaction between ACN and water, ^{1}H NMR of a salt-free ACN–water mixture (PACN50, 50 wt% ACN) was also investigated as shown in Fig. 3c. Note that the ^{1}H peak of H_2O in PACN-50 is at 4.634 ppm which is different from ACN-50 with a $\Delta\sigma \approx 0.004$ ppm, indicating that adding salt affects the hydrogen-bonding interaction of ACN and water, and that ACN can participate in the cationic solvation by replacing the water molecules in the solvation sheath (Fig. 3d). These interactions among ACN, H_2O and salts are benefit for inhibiting side reactions and extending electrochemical window of the aqueous batteries.

To explore the potential application of the hybrid electrolyte in aqueous batteries, FeHCF||Zn full cells were assembled with the ACN-0, ACN-25 and ACN-50 electrolytes because of their inflammable feature, and acceptable ionic conductivity and viscosity. Fig. 4a–c show the charge–discharge curves of the aqueous batteries at 1C (100 mA g^{-1}) between 0.6 and 1.5 V. The initial discharge capacities of the batteries with ACN-0, ACN-25 and ACN-50 are 73.5, 76.2 and 77.2 mA h g^{-1}, with coulombic efficiencies of 89.5%, 88.9% and 88.7%, respectively. Namely, the addition of ACN can increase the capacity of the FeHCF||Zn cell. Note that the battery with ACN-20 and ACN-50 also exhibits higher average discharge voltage than that with ACN-0 (1.04 V

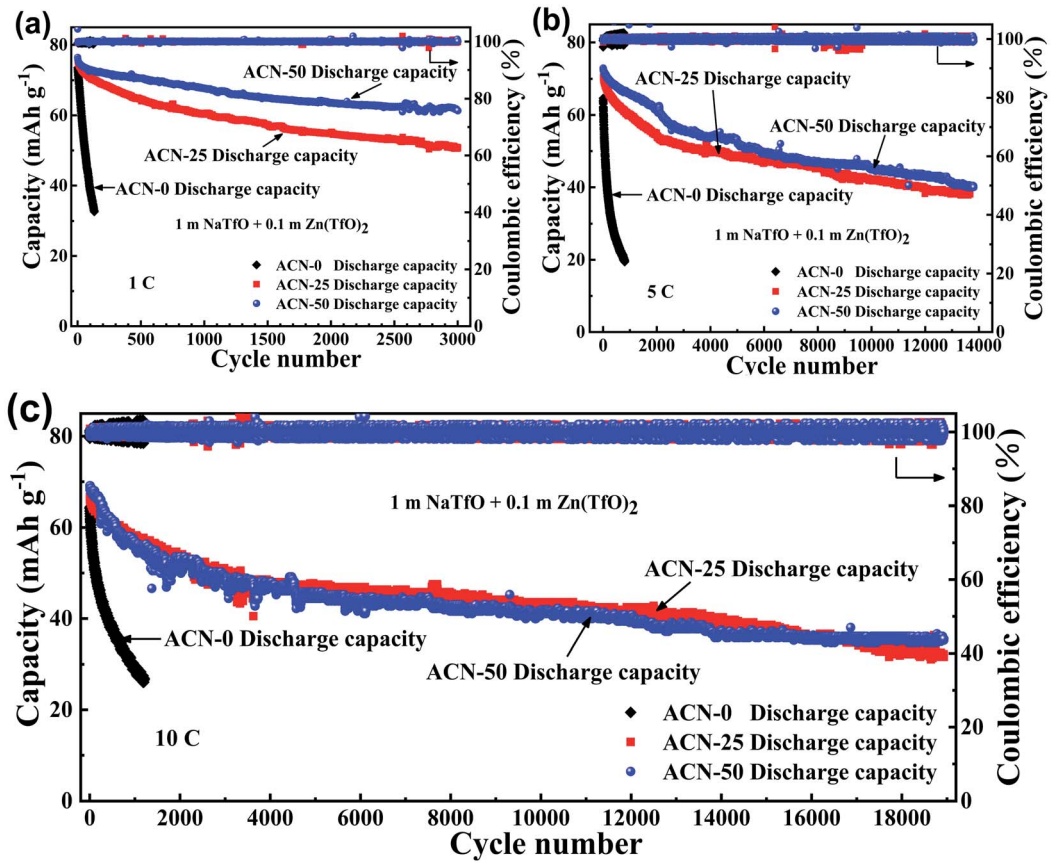

Fig. 5 Cycle stability for AB-0, AB-25 and AB-50 aqueous batteries at different current density: (a) 1C, (b) 5C and (c) 10C.

vs. 0.98 V), suggesting high energy density of the batteries using the hybrid electrolytes. The lower discharge capacity and larger polarization for the ACN-0 battery compared to the ACN-25 and ACN-50 batteries are due to the increased side reactions and sluggish insertion reaction of Na^+ into FeHCFs owing to the high activity of free H_2O without adding ACN. At the fifth cycle, the coulombic efficiency of the ACN-20 and ACN-50 batteries increases to nearly 100%, higher than that of the ACN-0 battery (99.4%), indicating inhibited parasitic reactions by adding ACN to reduce H_2O decomposition.

Fig. 5 compares the cycle performance of the FeHCF||Zn cells with ACN-0, ACN-25 and ACN-50 hybrid electrolytes at 1C. Although the batteries deliver a similar initial capacity, their cycling stability differs significantly. The ACN-0 aqueous battery suffers from a rapid capacity decay with only 44.2% capacity retention after 130 cycles, while the ACN-20 and ACN-50 batteries exhibit better cycling stability with 66.5% and 80.4% capacity retention after 3000 cycles (Fig. 5a). The improved cycling stability of the batteries using the hybrid electrolytes is attributed to the formation of stronger hydrogen bonds between ACN and H_2O to reduce the activity of water with inhibited side reactions. The batteries were cycled at higher current densities of 5C and 10C to check the rate capability and high-rate cycling stability as seen in Fig. 5b and c. The initial discharge capacities of the ACN-0, ACN-25 and ACN-50 are 64.6, 70.5 and 72.9 mA h g^{-1}, respectively, at 5C, and 64.2, 66.6 and 69.1 mA h g^{-1}, respectively, at 10C. The results reveal that the rate performance is not significantly affected with increasing ACN ratio. However, the cycling stability of the aqueous batteries can be obviously enhanced by introducing ACN. The ACN-0 battery suffers from a rapid capacity fade with only 30.9% retention after 800 cycles at 5C and 41.1% retention after 1200 cycles at 10C. In contrast, the ACN-25 and ACN-50 batteries show an excellent cycling stability at 5C, sustaining an ultralong cycle life of 14 000 cycles with 54.2% and 55.4% retention, respectively. At 10C current density, 47.4% and 51.4% capacity retention can also be obtained for the ACN-25 and ACN-50 batteries after 19 000 cycles. Clearly, the ACN plays a critical role in improving cycling stability of the aqueous batteries especially at high current density. In order to evaluate the electrochemical performance of our FeHCF/Zn batteries using ACN-50 hybrid aqueous electrolyte, we compare the cycle life and discharge capacity with various battery systems as shown in Table S1 (ESI†). Note that although our aqueous FeHCF/Zn batteries exhibit inferior cycling performance compared to those using solid electrolyte because of more severe side reactions, and dissolution/corrosion of the electrode materials,[35,36] the FeHCF/Zn batteries generally have a longer cycle life compared with those using also aqueous electrolytes or bare organic electrolyte.[37–40] Considering the practical applications of the aqueous FeHCF/Zn batteries, we also studied the gas evolution experiments of the battery in the idle mode as shown

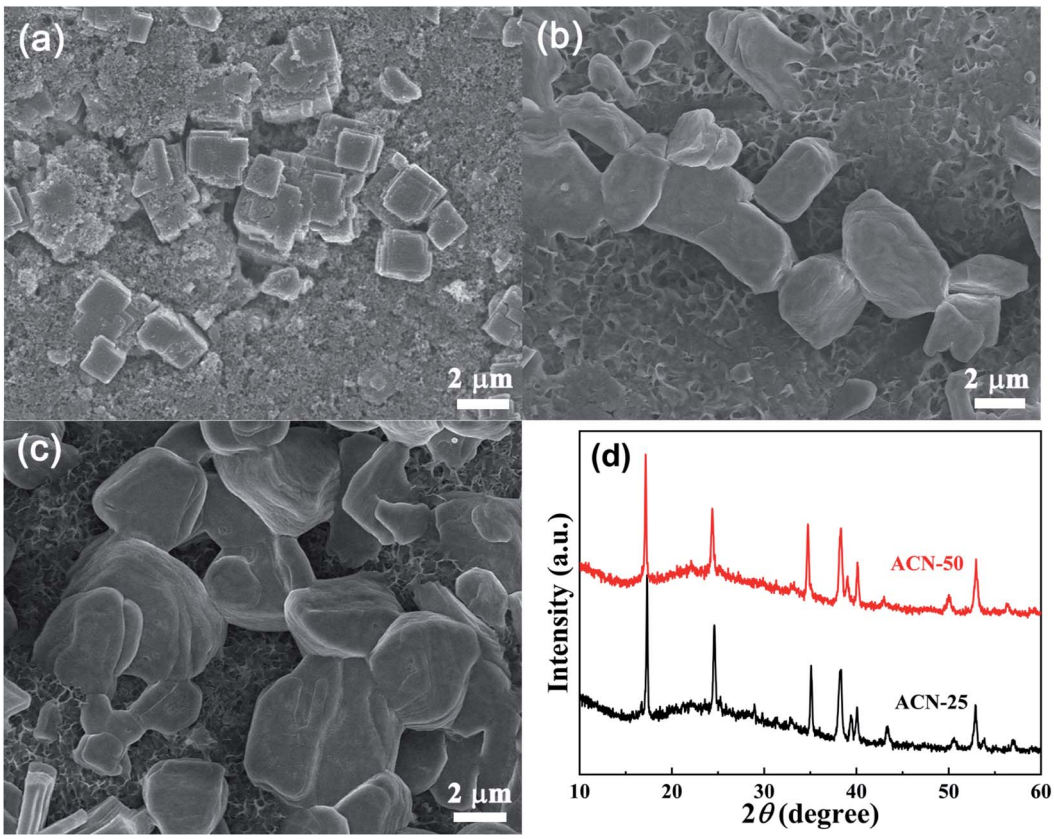

Fig. 6 SEM image of the FeHCF electrodes of (a) pristine, (b) after 19 000 cycles in ACN-25 and (c) after 19 000 cycles in ACN-50, and (d) XRD patterns of the FeHCF electrodes after 19 000 cycles in ACN-25 and ACN-50.

in Fig. S1 (ESI†). Note that no obvious gas evolution occurs on either FeHCF cathode or Zn anode at charge or discharge state, which further demonstrates that the FeHCF/Zn battery with the ACN/H_2O hybrid electrolyte can be potentially applied in large-scale energy storage.

To further understand the superior cycling performance of the FeHCF/Zn batteries, SEM and XRD characterizations were performed on the electrodes after 19 000 cycles at 10C in the hybrid electrolyte as shown in Fig. 6. It can be seen that the pristine sharp corners of FeHCF cubes become smooth with the multi-edge structure disappeared. The structural changes agree with the gradual capacity decay of the material after long-term cycling. However, the material does not suffer from severe dissolution and corrosion, which is consistent with the superior cycling stability of the aqueous batteries (Fig. 6b and c). Fig. 6d shows the XRD patterns of the FeHCF electrodes after 19 000 cycles at 10C. The sharp diffraction peaks indicate that the high crystallinity of the FeHCF material is still well preserved after repeated cycling, also agreeing with the excellent cycling stability. Note that the crystal structure is changed from monoclinic to cubic phase.

4. Conclusion

In summary, a hybrid aqueous electrolyte composed of ACN and H_2O has been proposed for aqueous FeHCF/Zn batteries. The addition of ACN can extend the electrochemical window at a normal salt concentration. By optimizing the ACN/H_2O ratio, the hybrid electrolyte has a combined merit of low cost, nonflammability, and reasonable viscosity and ionic conductivity. The stronger hydrogen-bonding interaction of ACN and H_2O than that of H_2O and H_2O helps for reorganizing the hydrogen-bond network with reduced water activity, so as to extend the electrochemical window of the aqueous electrolytes, with inhibited electrode corrosion/dissolution and side reactions. The aqueous FeHCF/Zn battery exhibits an impressively long cycle life with 51.4% capacity retention after 19 000 cycles at 10C by using a hybrid solvent with a relatively high ACN ratio (50 wt%, ACN-50) while still keeping nonflammable. In sharp contrast, the battery with bare water solvent (ACN-0) shows an obviously inferior cycling stability (41.1% retention after only 1200 cycles). The aqueous batteries with 50 wt% ACN addition also exhibit superior rate capability comparing to ACN-0 and deliver a higher capacity of 69.1 mA h g^{-1} at 10C (89.5% retention relative to 1C). Besides the advantages of the aqueous electrolyte, the open framework of Prussian material, the large particle size of the FeHCF, and the multi-edge structure also contribute to the outstanding rate capability and extremely long cycle life. This work provides a practical design of aqueous batteries with potential applications in large-scale energy storage.

Conflicts of interest

There are no conflicts to declare.

Acknowledgements

This work was supported by Major Science and Technology Project of Hunan Province (2020GK1014), joint research project of Zhejiang University and LI-FUN Technology Corporation limited, and joint research project of Zhejiang University and Huayou New Energy Technology (Quzhou) Co., Ltd.

References

1 B. Dunn, H. Kamath and J. M. Tarascon, *Science*, 2011, **334**, 928–935.
2 A. R. Dehghani Sanij, E. Tharumalingam, M. B. Dusseault and R. Fraser, *Renewable Sustainable Energy Rev.*, 2019, **104**, 192–208.
3 T. M. Gür, *Energy Environ. Sci.*, 2018, **11**, 2696–2767.
4 K. Chayambuka, G. Mulder, D. L. Danilov and P. H. L. Notten, *Adv. Energy Mater.*, 2020, **10**, 2001310.
5 K. Chayambuka, G. Mulder, D. L. Danilov and P. H. L. Notten, *Adv. Energy Mater.*, 2018, **8**, 1800079.
6 J. Kalhoff, G. G. Eshetu, D. Bresser and S. Passerini, *ChemSusChem*, 2015, **8**, 2154–2175.
7 Z. Yang, X. H. Liu, X. X. He, W. H. Lai, L. Li, Y. Qiao, S. L. Chou and M. H. Wu, *Adv. Funct. Mater.*, 2020, **31**, 2006457.
8 K. V. Kravchyk, M. Walter and M. V. Kovalenko, *Commun. Chem.*, 2019, **2**, 84.
9 X. G. Sun, Z. Z. Zhang, H. Y. Guan, C. A. Bridges, Y. X. Fang, Y. S. Hu, G. M. Veith and S. Dai, *J. Mater. Chem. A*, 2017, **5**, 6589–6596.
10 G. L. Li, Z. Yang, Y. Jiang, W. X. Zhang and Y. H. Huang, *J. Power Sources*, 2016, **308**, 52–57.
11 Z. G. Hou, X. Q. Zhang, X. N. Li, Y. C. Zhu, J. W. Liang and Y. T. Qian, *J. Mater. Chem. A*, 2017, **5**, 730–738.
12 X. W. Wu, Y. H. Li, Y. H. Xiang, Z. X. Liu, Z. Q. He, X. M. Wu, Y. J. Li, L. Z. Xiong, C. C. Li and J. Chen, *J. Power Sources*, 2016, **336**, 35–39.
13 K. Lu, B. Song, J. T. Zhang and H. Y. Ma, *J. Power Sources*, 2016, **321**, 257–263.
14 D. Bin, F. Wang, A. G. Tamirat, L. M. Suo, Y. G. Wang, C. S. Wang and Y. Y. Xia, *Adv. Energy Mater.*, 2018, **8**, 1703008.
15 Z. X. Liu, Y. Huang, Y. Huang, Q. Yang, X. L. Li, Z. D. Huang and C. Y. Zhi, *Chem. Soc. Rev.*, 2020, **49**, 180–232.
16 H. Kim, J. Hong, K. Y. Park, H. Kim, S. W. Kim and K. Kang, *Chem. Rev.*, 2014, **114**, 11788–11827.
17 Y. Y. Wang, X. T. Meng, J. F. Sun, Y. Liu and L. R. Hou, *Front. Chem.*, 2020, **8**, 595.
18 D. L. Chao and S. Z. Qiao, *Joule*, 2020, **4**, 1846–1851.
19 O. Borodin, J. Self, K. A. Persson, C. S. Wang and K. Xu, *Joule*, 2020, **4**, 69–100.
20 W. Sun, L. M. Suo, F. Wang, N. Eidson, C. Y. Yang, F. D. Han, Z. H. Ma, T. Gao, M. Zhu and C. S. Wang, *Electrochem. Commun.*, 2017, **82**, 71–74.
21 M. H. Lee, S. J. Kim, D. Chang, J. Kim, S. Moon, K. Oh, K. Y. Park, W. M. Seong, H. Park, G. Kwon, B. Lee and K. Kang, *Mater. Today*, 2019, **29**, 26–36.
22 S. R. Chen, J. M. Zheng, L. Yu, X. D. Ren, M. H. Engelhard, C. J. Niu, H. Lee, W. Xu, J. Xiao, J. Liu and J. G. Zhang, *Joule*, 2018, **2**, 1548–1558.

23 S. R. Chen, J. M. Zheng, D. H. Mei, K. S. Han, M. H. Engelhard, W. G. Zhao, W. Xu, J. Liu and J. G. Zhang, *Adv. Mater.*, 2018, **30**, 1706102.
24 J. Zheng, G. B. Ji, X. L. Fan, J. Chen, Q. Li, H. Y. Wang, Y. Yang, K. C. DeMella, S. R. Raghavan and C. S. Wang, *Adv. Energy Mater.*, 2019, **9**, 1803774.
25 N. N. Chang, T. Y. Li, R. Li, S. N. Wang, Y. B. Yin, H. M. Zhang and X. F. Li, *Energy Environ. Sci.*, 2020, **13**, 3527–3535.
26 J. Xie, Z. J. Liang and Y. C. Lu, *Nat. Mater.*, 2020, **19**, 1006–1011.
27 Q. S. Nian, J. Y. Wang, S. Liu, T. J. Sun, S. B. Zheng, Y. Zhang, Z. L. Tao and J. Chen, *Angew. Chem., Int. Ed.*, 2019, **58**, 16994–16999.
28 J. Q. Shi, K. X. Xia, L. J. Liu, C. Liu, Q. Zhang, L. Li, X. Z. Zhou, J. Liang and Z. L. Tao, *Electrochim. Acta*, 2020, **358**, 136937.
29 D. W. Xiao, Q. Y. Dou, L. Zhang, Y. L. Ma, S. Q. Shi, S. L. Lei, H. Y. Yu and X. B. Yan, *Adv. Funct. Mater.*, 2019, **29**, 1904136.
30 C. L. Liu, Y. P. Sun, J. B. Nie, D. Dong, J. Xie and X. B. Zhao, *New J. Chem.*, 2020, **44**, 4639–4646.
31 Z. M. Zhao, J. W. Zhao, Z. L. Hu, J. D. Li, J. J. Li, Y. J. Zhang, C. Wang and G. L. Cui, *Energy Environ. Sci.*, 2019, **12**, 1938–1949.
32 Z. L. Shen, S. H. Guo, C. L. Liu, Y. P. Sun, Z. Chen, J. Tu, S. Y. Liu, J. P. Cheng, J. Xie, G. S. Cao and X. B. Zhao, *ACS Sustainable Chem. Eng.*, 2018, **6**, 16121–16129.
33 X. W. Cao, N. Gong, H. L. Zhao, Z. W. Li, C. L. Sun and Z. W. Men, *J. Mol. Liq.*, 2019, **279**, 625–631.
34 Q. S. Nian, X. R. Zhang, Y. Z. Feng, S. Liu, T. J. Sun, S. B. Zheng, X. D. Ren, Z. L. Tao, D. H. Zhang and J. Chen, *ACS Energy Lett.*, 2021, **6**, 2174–2180.
35 L. T. Ma, S. M. Chen, X. L. Li, A. Chen, B. B. Dong and C. Y. Zhi, *Angew. Chem., Int. Ed.*, 2020, **59**, 23836–23844.
36 L. T. Ma, S. M. Chen, N. Li, Z. X. Liu, Z. J. Tang, J. A. Zapien, S. M. Chen, J. Fan and C. Y. Zhi, *Adv. Mater.*, 2020, **32**, 1908121.
37 D. H. Wang, H. M. Lv, T. Hussain, Q. Yang, G. J. Liang, Y. W. Zhao, L. T. Ma, Q. Li, H. F. Li, B. B. Dong, T. Kaewmaraya and C. Y. Zhi, *Nano Energy*, 2021, **84**, 105945.
38 A. Naveed, H. J. Yang, J. Yang, Y. Nuli and J. L. Wang, *Angew. Chem., Int. Ed.*, 2019, **58**, 2760–2764.
39 N. Zhang, Y. Dong, Y. Y. Wang, Y. X. Wang, J. J. Li, J. Z. Xu, Y. C. Liu, L. F. Jiao and F. Y. Cheng, *ACS Appl. Mater. Interfaces*, 2019, **11**, 32978–32986.
40 W. Kao. Ian, R. Pornprasertsuk, P. Thamyongkit, T. Maiyalagan and S. Kheawhom, *J. Electrochem. Soc.*, 2019, **166**, A1063–A1069.